Supporting Information

Defect-Engineered MOF-808 for Catalytic Transfer Hydrogenation of Furfural: Structural Insights from Comparative Studies

Xiao Ma,[a] Hongyang Yu[b], Yu Zhang[b], Chang Sun,[a] Chang Gong,[a] Ting Xu,[a] Cuiqin Li,[a] Feng Li [a, *]

[a] College of Chemistry & Chemical Engineering, Northeast Petroleum University, Daqing163318, Heilongjiang, China

[b] North Huajin Chemical Industries Group Corporation, Panjin 124021, Liaoning, China

[*] Corresponding author.
E-mail address: lifeng@nepu.edu.cn (F. Li)

Materials

Zirconyl chloride octahydrate ($ZrOCl_2 \cdot 8H_2O$), 1,3,5-benzenetricarboxylic acid (H_3BTC), 1,3-benzenedicarboxylic acid (H_2BDC), benzoic acid (HBC), N,N′-dimethylformamide (DMF), formic acid, methanol, ethanol, FAL, and *i*-propanol were purchased from Aladdin Biochemical Technology Co., Ltd. All reagents were used as received without further purification.

Catalyst characterization

X-ray diffraction (XRD) patterns were recorded on a Rigaku SmartLab SE diffractometer with Cu Kα radiation. Scanning electron microscopy (SEM) images were acquired using a Zeiss SIGMA microscope. N_2 adsorption-desorption isotherms were measured using a Micromeritics ASAP 2460 surface area analyzer. Fourier transform infrared (FTIR) spectra were collected on a Nicolet 5700 spectrometer. Thermogravimetric (TG) analysis was performed on a TA SDT-Q600 analyzer from 30 to 700 ℃ at 10 ℃·min^{-1} under air. X-ray photoelectron spectroscopy (XPS) was conducted on a Thermo Fisher Scientific spectrometer with monochromatic Al Kα radiation (E=1486.6 eV). NH_3 and CO_2 temperature-programmed desorption (NH_3/CO_2-TPD) analyses were performed using a Micromeritics AutoChem II 2920 chemisorption analyzer. Pyridine-FTIR (Py-FTIR) spectroscopy was carried out on a Nicolet 5700 spectrometer to identify acid site types.

Catalytic tests

CTH of FAL was performed in a 50 mL stainless steel reactor with magnetic stirring. Typically, 10 mmol FAL, 20 mg catalyst, and 10 mL *i*-propanol were loaded into the reactor, which was then purged with N_2 to remove air. The mixture was stirred at 180 ℃ for 1 h. After

reaction, liquid products were collected by centrifugation and analyzed via gas chromatography (GC-14C, Shimadzu) with flame ionization detection.

Table S1 Textural properties of MOF-808, MOF-808-II_{10} and MOF-808-I_{40}.

Samples	S_{BET} ($m^2 \cdot g^{-1}$)	V_{pore} ($cm^3 \cdot g^{-1}$)	d_{pore} (nm)
MOF-808	1161.81	0.50	2.21
MOF-808-II_{10}	1161.74	0.41	1.89
MOF-808-I_{40}	754.07	0.27	1.92

Table S2 Spectral fitting parameters of two types of oxygen groups for MOF-808, MOF-808-II_{10} and MOF-808-I_{40}.

Samples	Zr–O–Zr	Zr–O–C	Ratios
	(Area %)	(Area %)	(Zr–O–C/Zr–O–Zr)
MOF-808	4.26	95.74	22.5:1
MOF-808-II_{10}	5.06	94.94	18.8:1
MOF-808-I_{40}	6.50	93.50	14.4:1

Table S3. Number of ligand defects of MOF-808 and its derivatives[a].

Samples	Weight (% ZrO_2)	Linkers	Miss linkers
MOF-808	191.6	6	0
MOF-808-II_{10}	187.7	5.88	0.12
MOF-808-II_{20}	182.9	5.73	0.27
MOF-808-II_{30}	178.5	5.59	0.41
MOF-808-II_{40}	172.9	5.42	0.58
MOF-808-I_{10}	183.9	5.76	0.24
MOF-808-I_{20}	179.5	5.62	0.38
MOF-808-I_{30}	173.5	5.43	0.57
MOF-808-I_{40}	169.0	5.29	0.71

[a] Calculated at 350 °C

Table S4. Catalytic performance of this work compared to other literatures.

Entry	Catalyst	FAL	Catalyst	N_2	Temp.	Time	C_{FAL}	S_{FOL}	Ref.
		(mmol)	(mg)	(MPa)	(K)	(h)	(%)	(%)	
1	MOF-808	10.4	100	—	355	2	81.3	81.7	[1]
2	D_{40}-MOF-808	10.4	100	—	363	2	99.0	94.4	[2]
3	A-MOF-801-64	1.0	100	—	403	12	99.0	98.0	[3]
4	HE-UiO-66	0.17	25	—	393	3	95.0	91.5	[4]
5	Zr@C-T	1	60	1	423	1.5	98.1	93.1	[5]
6	DUT-52	3	75	—	433	3	>99	>99	[6]
7	meso-Zr-glu	2	50	—	453	3	99.1	94.2	[7]
8	ZrMg@Fe_3O_4	4	200	—	463	5	99.1	93.3	[8]
9	Zr-20@PAN	3.1	100	—	423	2	98.4	91.8	[9]
10	Pt@Zr-SBTD-NH_2	1	30	1.5	393	3	98	97	[10]
11	Pd-Cu/MCM-41	1.8	60	—	433	4	97.4	98.3	[11]
12	Cu/Zn@NC-T	1.0	50	1	433	2	100	96.78	[12]
13	HfO_x@ZSM-5	3.12	200	—	433	1	>99	>99	[13]
14	MOF-808	10	10	1	453	1	72.9	92.8	This work
15	MOF-808-I_{40}	10	10	1	453	1	94.7	95.4	This work

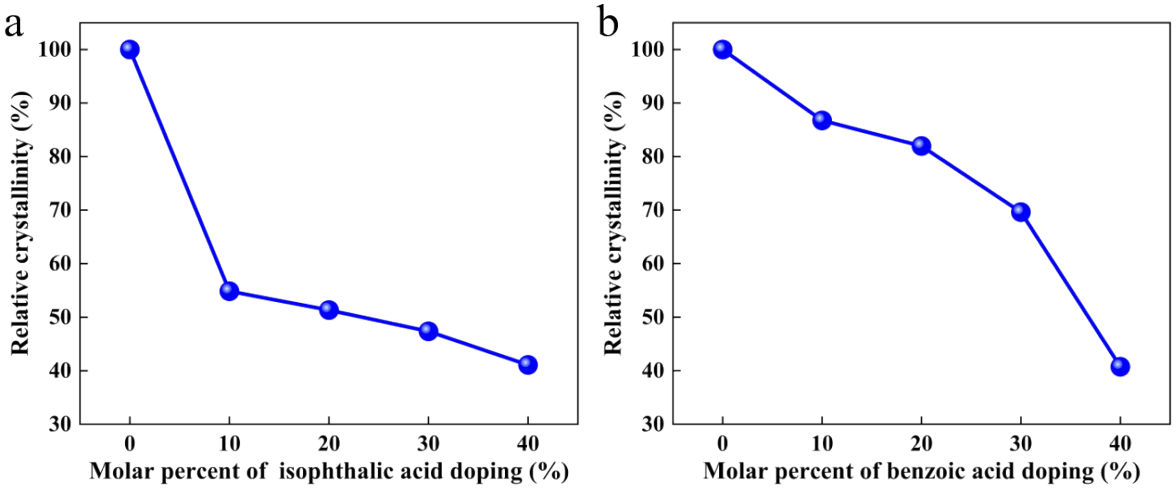

Figure S1. Relative crystallinity of (a) MOF-808-II_x and (b) MOF-808-I_y.

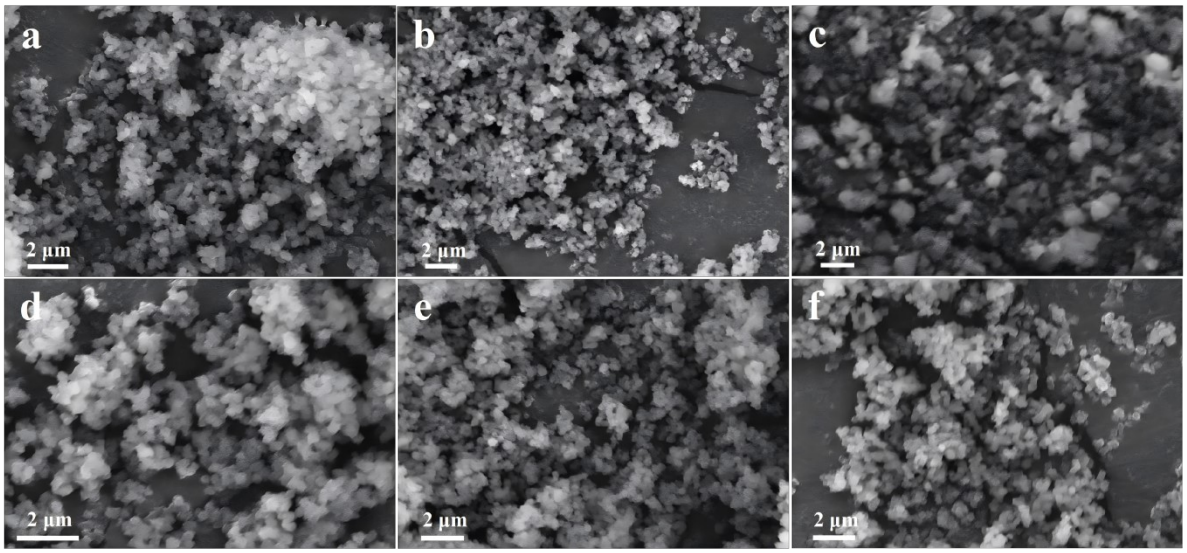

Figure S2. SEM images of (a) MOF-808-II_{20}, (b) MOF-808-II_{30}, (c) MOF-808-II_{40}, (d) MOF-808-I_{10}, (e) MOF-808-I_{20} and (f) MOF-808-I_{30}.

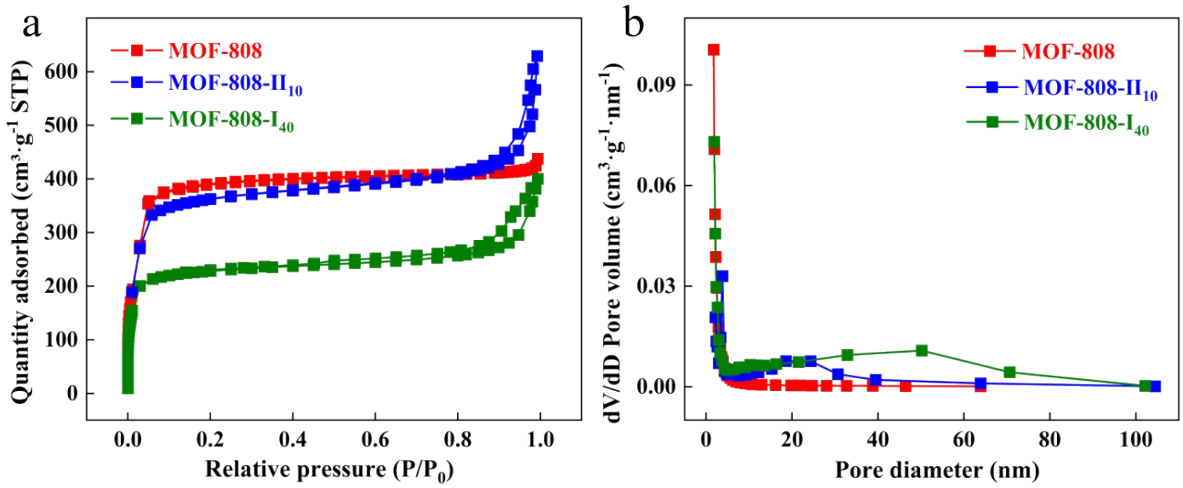

Figure S3. (a) N_2 adsorption–desorption isotherms and (b) pore-size distribution of MOF-808, MOF-808-II_{10} and MOF-808-I_{40}.

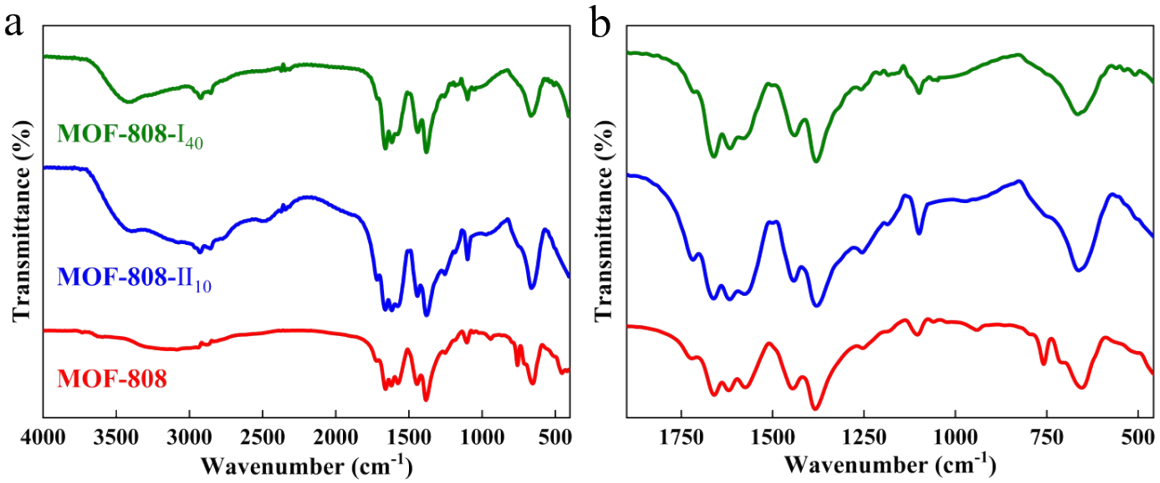

Figure S4. FTIR spectra of MOF-808, MOF-808-II_{10} and MOF-808-I_{40}.

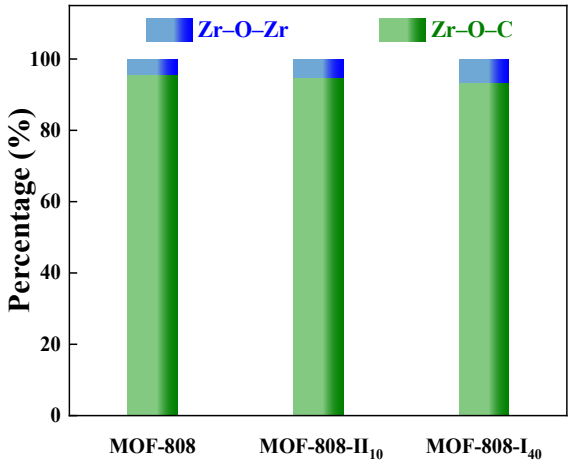

Figure S5. The contents of two types of oxygen groups calculated from the peak area of two types of oxygen (Zr–O–Zr and Zr–O–C refer to the bridged O group on SBUs and the coordinated carboxylate groups, respectively).

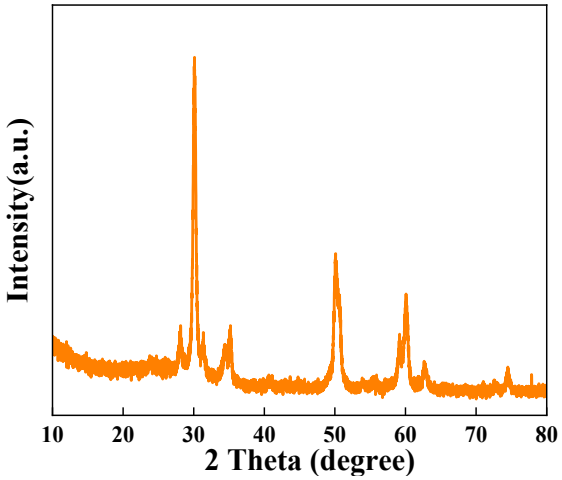

Figure S6. XRD pattern of MOF-808 calcined at 700 ℃ under air.

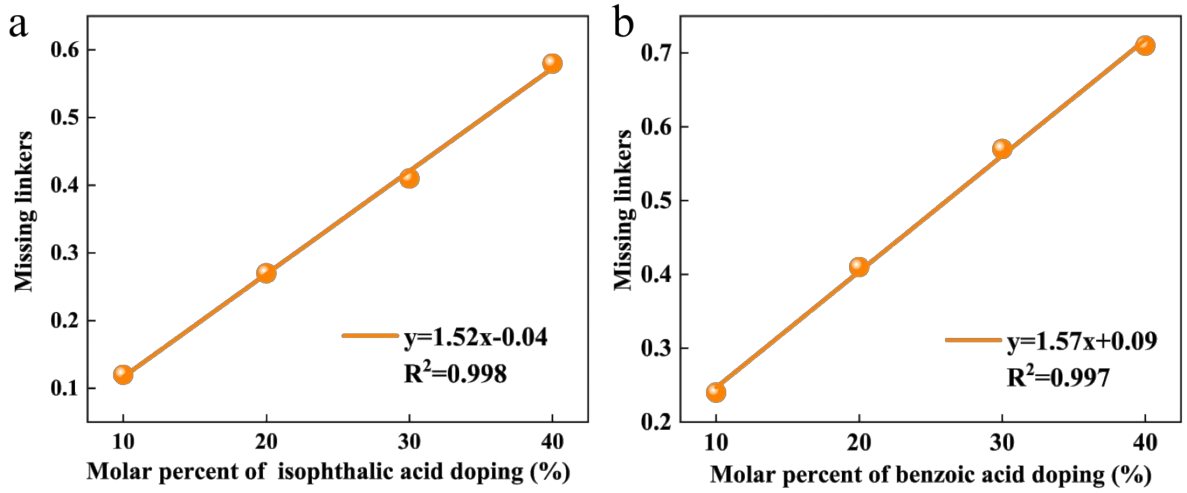

Figure S7. (a) Relationship between H_2BDC molar percent and missing linkers of MOF-808-II_x and (b) relationship between HBC molar percent and missing linkers of MOF-808-I_y.

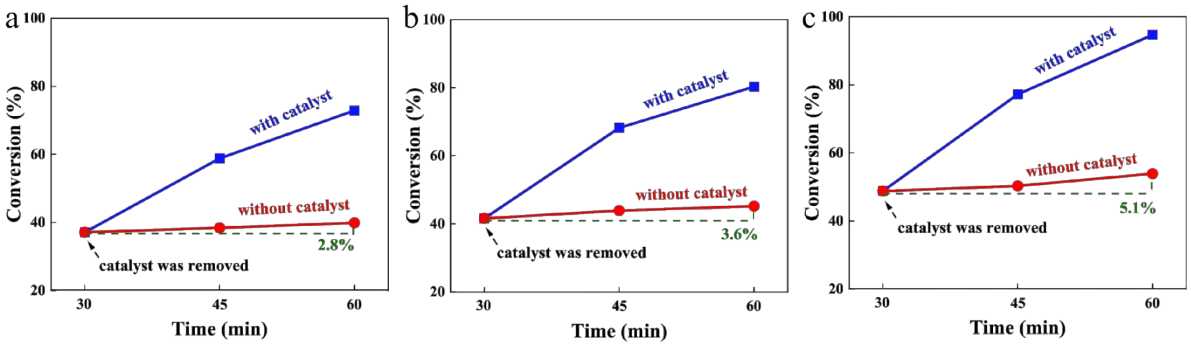

Figure S8. Hot filtration test (a) MOF-808 (b) MOF-808-II_{10} and(c)MOF-808-I_{40}. Reaction conditions: 20 mg of catalyst, 10 mmol of FAL, 10 mL of *i*-propanol, 1 MPa N_2, 180 ℃..

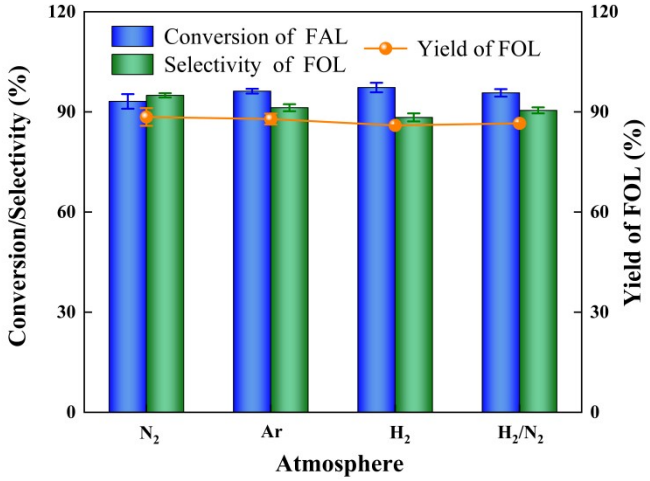

Figure S9. Under different atmosphere on FAL CTH over MOF-808-I_{40}. Reaction conditions: 20 mg of catalyst, 10 mmol of FAL, 10 mL of *i*-propanol, 1 MPa atmosphere, 180 ℃, 1 h.

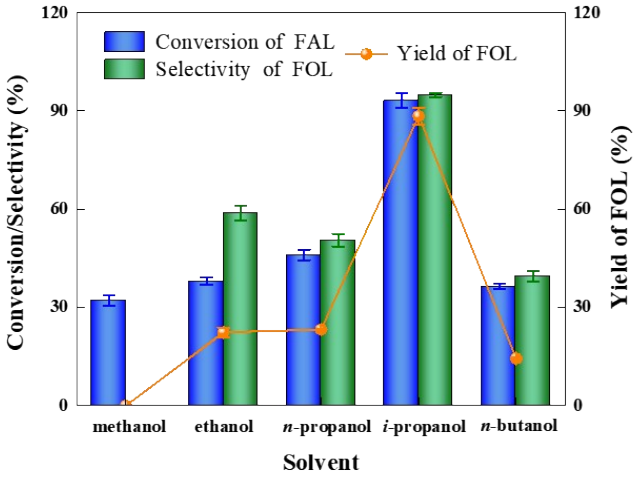

Figure S10. Under different solvent on FAL CTH over MOF-808-I_{40}. Reaction conditions: 20 mg of catalyst, 10 mmol of FAL, 10 mL of solvent, 1 MPa N_2, 180 ℃, 1 h.

I-propanol is the optimal hydrogen donor. From the perspective of reduction potential, the reduction potentials of various alcohols rank as follows: *i*-propanol (70.0 kJ·mol^{-1}) < *n*-butanol (79.7 kJ·mol^{-1}) < ethanol (85.4 kJ·mol^{-1}) < *n*-propanol (87.3 kJ·mol^{-1}) < methanol (130.1 kJ·mol^{-1}) [2]. The secondary have lower reduction potentials than primary alcohols. The lower reduction potentials, the stronger dehydrogenation capability. From the perspective of hydrophilicity and steric effect, the longer carbon chains diminish hydrophilic adsorption on active sites and reduce conversion efficiency via steric hindrance [14].

References

1 A. Valekar, M. Lee, J. Yoon, J. Kwak, D. Hong, K. Oh, G. Cha, Y. Kwon, J. Jung and J. Chang, *ACS Catal.*, 2020, **10**, 3720–3732.

2 Q. Fu, D. Liu, W. Niu, S. Zhang, R. Chen, Y. Wang and X. Zhao, *Fuel*, 2022, **327**, 125085.

3 Y. Liu, Q. Fu, W. Niu, Y. Zhang, W. Xie, H. Jiang, L. Yan, G. Li and X. Zhao, *Molecules*, 2025, **30**, 2697.

4 M. Ma, E. Chen, H. Yue, G. Tian and S. Feng, *Nat. Commun.*, 2025, **16**, 367.

5 Y. Qiu, Y. Shui, H. Liu, R. Shan, J. Zhang, J. Zhang and H. Yuan, *J. Energy Inst*., 2025, **121**, 102163.

6 K. Agusta, M. Miharja, A. Sakti, U. Arrozi, L. Mukaromah, A. Patah, T. Hara and Y. Permana, *Mol. Catal.*, 2022, **524**, 112265.

7 J. Yang, Y. Zhang, F. Shen and X. Qi, *Biomass Bioenergy*, 2023, **170**, 106723.

8 J. Qiu, B. Zhou, Q. Yang, Y. Liu, L. Zhang, B. Wang, S. Song, J. Zhang, S. Huang, J. Chen, L. Lin and X. Zeng, *Fuel Process. Technol*., 2024, **254**, 108010.

9 W. Lin, Y. Cheng, H. Liu, J. Zhang and L. Peng, *Fuel*, 2023, **331**, 125792.

10 K. Tong, G. Lu, F. Kong, Z. Wei, Z. Zhan and X. Wang, *ACS Appl. Nano Mater*., 2025, **8**, 17440–17450.

11 B. Gao, J. Zhang, M. Zhang, H. Li and J. Yang, *Appl. Surf. Sci*., 2023, **619**, 156716.

12 Y. Cheng, Z. Mo, H. Liu, C. Wang and Z. Zhang, *J. Phys. Chem. C*, 2025, **129**, 4323–4332.

13 F. Chen, T. Lv, W. Jia, H. Liu, R. Zhang, L. Peng and J. Zhang, *Mol. Catal*., 2025, **584**, 115315.

14 S. Kumaravel, J. Alagarasan, A. Yadav, W. Ali, M. Lee, M. Khan, S. Ali, A. Bashiri, W.

Zakri and K. Balu, *J. Phys. Chem. Solids*, 2024, **186**, 111831.